

Modeling of component failure due to notch effects in press-hardened steel caused by mechanical and thermo-mechanical joints under crash load

Philipp Bähr¹, Silke Sommer¹, Eduard Unruh², Gerson Meschut²

¹Fraunhofer - Institute for Mechanics of Materials IWM
Wöhlerstraße 11, 79108 Freiburg, Germany

²Laboratory for Materials and Joining Technology (LWF), University of Paderborn
Pohlweg 47-49, 33098 Paderborn, Germany

1 Introduction

The increasing application of press-hardened steel in combination with aluminum sheets in the construction of car bodies results in the use of mechanical joining techniques such as self-piercing riveting and thermo-mechanical joining techniques such as resistance element welding. These joints generally represent a notch within the component. The cause of the notch effect is different for the investigated joining techniques and can be distinguished in a geometrical notch and a metallurgical notch. Riveted joints result in a pierced hole with high plastic strains at the edge and thus represent a geometrical notch. Thermo-mechanical joints in press-hardened steel result in a softened heat affected zone (SHAZ) around the weld due to the applied heat during the joining process. Thus, they represent a metallurgical notch. A schematic representation of a geometrical notch can be found in Fig. 1a using the example of a tensile specimen with a central hole. In Fig. 1b, a spot weld with a surrounding heat affected zone is shown as an example for a metallurgical notch. All of these notch effects can be critical for the structural integrity of a component under crash load. Due to limited computational resources, a detailed modeling of joints within a component simulation is not possible. Thus, simplified modeling approaches such as the `*MAT_SPOTWELD_DAIMLER` [1] or the `*CONSTRAINED_SPR3` (model 2) [2] are applied in order to represent the load bearing capacity and failure behavior of the joints. These simplified models are usually used with shell elements for the sheet metals, whereby no notch effects such as pre-damage or differences in the microstructure are taken into consideration. Therefore, crack initiation in plane of the sheet metals due to these notch effects cannot be described in the simulation.

Subject of this research project is the development of a modeling approach that takes material failure due to notch effects at mechanical and thermo-mechanical joints into consideration. Two distinct approaches are developed for the two investigated notches. Both of the approaches are based on an explicitly modeled notch zone at the joint. For the mechanical joining techniques, a hole in the press-hardened steel is modeled, with an additionally defined pre-damage for the shell elements surrounding the hole. For the thermo-mechanical joints, a SHAZ with modified flow and failure behavior is modeled. The modeling approaches are calibrated based on experimental results of tensile and punch tests, which have been conducted with notched specimens. Additionally `*CONSTRAINED_SPR3` (model 2) models are calibrated based on the results of LWF-KS-2-specimens [3] in order to include the load bearing capacity and failure behavior of the joint itself. The generated models are validated based on experimental results of component tests, which have failed because of notches due to the investigated joining techniques.

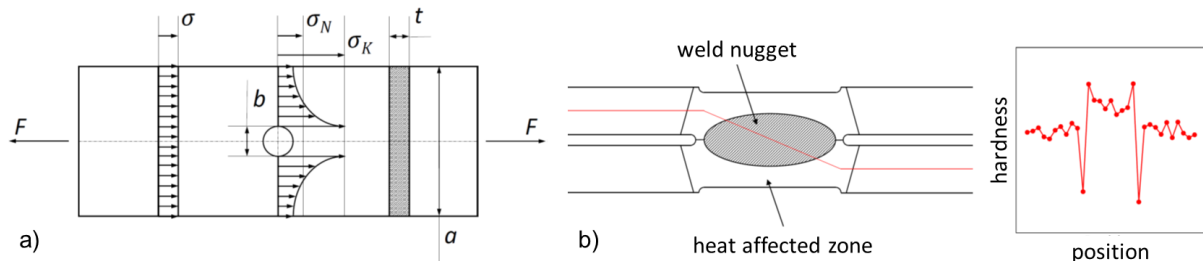


Fig. 1: a) Tensile specimen with a central hole as an example for a geometrical notch, b) Schematic cross section of a spot weld with weld nugget and heat affected zone as well as the corresponding hardness profile as an example for a metallurgical notch

2 Database

The experimental database for this paper originates from the AiF/FOSTA research project P1268 “Characterization and modeling of notch effects due to multi-material joints in car body components made of ultra-high strength steel” [4]. This project was carried out by the Fraunhofer - Institute for Mechanics of Materials IWM in cooperation with the Laboratory for Materials and Joining Technology (LWF) from the University of Paderborn. In this research project, notch effects due to mechanical and thermo-mechanical joints in press-hardened steel have been investigated experimentally and numerically. A sheet metal connection between 22MnB5 ($t = 1.5$ mm) and EN AW6016 ($t = 2.0$ mm) served as the basis for the investigation. An overview of some of the investigated specimen types can be found in Fig. 2. The LWF-KS-2 specimen, which can be seen in Fig. 2a, is a specimen that can be used for the characterization of joints under varying load angles [3]. A load angle of 0° corresponds to a shear loading of the joint. A load angle of 90° corresponds to a tensile load of the joint. The load angles 30° and 60° correspond to a mix of shear and tensile load. Furthermore, the load bearing capacity under peeling can be investigated with a modified version of the LWF-KS-2-specimen. For the characterization of the notch effects under in-plane load, a tensile and a punch specimen with a notch due to a joint in the middle of the specimen have been investigated (Fig. 2b). In this work, the results of the LWF-KS-2-specimens will be used in order to calibrate `*CONSTRAINED_SPR3` (model 2) models. The results of the tensile and punch specimens will be used to characterize the effect of notches due to joints under in-plane load for the numerical simulation.

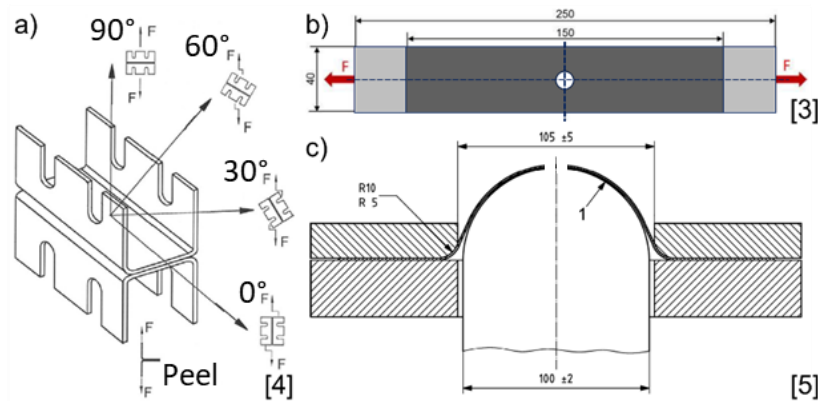


Fig.2: a) LWF-KS-2 specimen for joint characterization under varying load angles [5], b) tensile test with central hole [4], c) punch test with central hole [6]

The material model for the investigated press-hardened 22MnB5 steel is taken from the AiF/FOSTA research project P806 “Characterization and simplified modeling of the fracture behavior of spot welds from ultra-high strength steels for crash simulation with consideration of the effects of the joints on component behavior” [7]. This Project was carried out by the Fraunhofer - Institute for Mechanics of Materials IWM in cooperation with the Laboratory for Materials and Joining Technology (LWF) from the University of Paderborn and the Material Testing Institute (MPA) from the University of Stuttgart. The flow curve for the investigated 22MnB5 steel has been recalibrated for the current batch of material (Fig. 3a). The failure curve was used unchanged (Fig. 3b). The regularization curve for the consideration of the influence of the element edge length was slightly modified for coarser meshes (Fig. 3c).

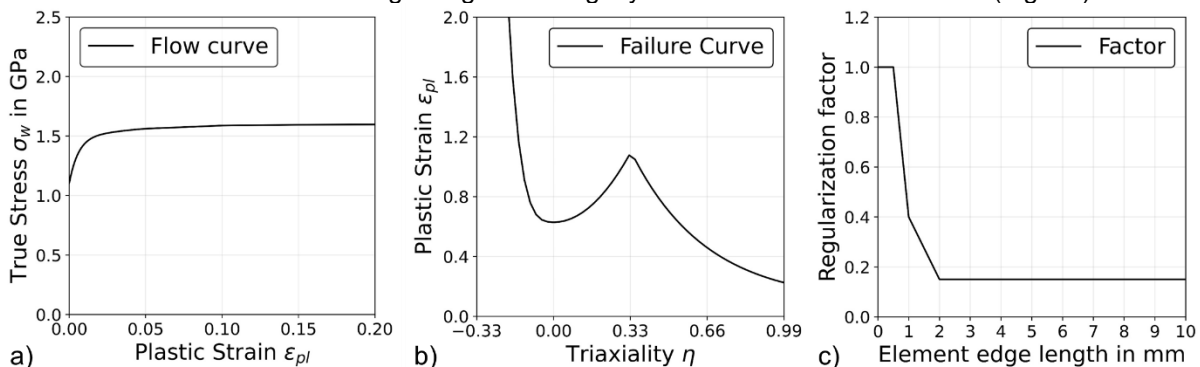


Fig.3: a) Flow curve, b) Failure curve and c) Regularization curve for the investigated press-hardened 22MnB5 steel [7]

3 Modeling of the joint behavior

In the following chapter, the developed approaches for the consideration of the experimentally observed notch effects in the modeling of joints is described. First, the approach for the geometrical notches is described, then the approach for the metallurgical notches. Both approaches are based on an explicitly modeled notch zone at the joint. The load bearing capacity of the joint itself is modeled with the ***CONSTRAINED_SPR3** (model 2) model. All the simulations shown in this chapter were executed with fully integrated shell elements (ELFORM=16) with a characteristic edge length of 1.5 mm near the joint. Material failure for the press-hardened steel was taken into account with the GISSMO damage model (***MAT_ADD_EROSION**) and the failure curve shown in Fig. 3b.

3.1 Geometrical notch at self-piercing rivets

The approach followed in this work to account for the geometric notch effect due to mechanical joining processes (self-piercing riveting) is based on an explicitly modeled notch zone for which a pre-damage value is defined. In this chapter, the procedure, which has been used to determine this pre-damage value, will be described. For the following investigations, the experimental results of the tensile and punch tests with a central hole due to self-piercing riveting have been used for calibration. First off all, shell models for the tensile and punch specimens have been created with an explicitly modeled hole with a surrounding notch zone in the middle of the specimen (Fig. 4). The diameter of the modeled hole corresponds to the real diameter of the self-piercing rivet. These models have been simulated with the damage model switched off in order to be able to evaluate the load paths of the critical elements within the notch zones. The results of these simulations can be seen in Fig. 5a. The red and blue line represent the load paths of the critical elements for the tensile and punch specimen, the black line represents the failure curve of the base material regularized according to the edge length of the critical element. The upper dots on the load path in Fig. 5a show the load at which failure would occur without the consideration of any pre-damage within the critical element. The lower dots on the load path the load at which failure has to occur in order to match the global behavior of the experimental specimens. Based on these results the value of the predefined damage can be calculated. The procedure for this will be described in the next section.

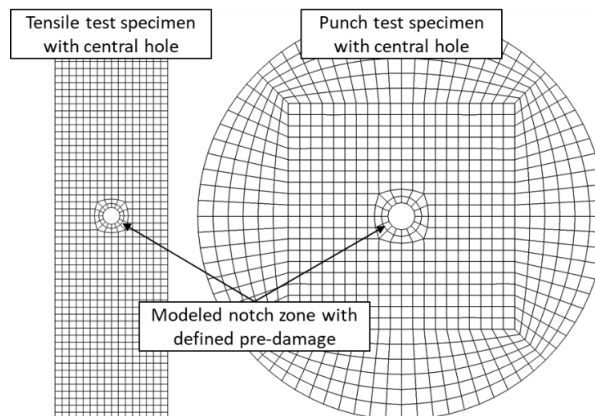


Fig.4: FE-models of the tensile and punch tests with a central hole due to self-piercing riveting

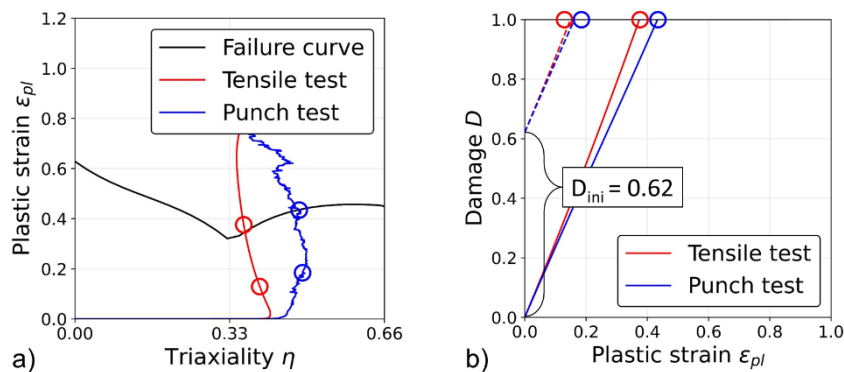


Fig.5: a) Load paths of the critical elements for the tensile and punch tests as well as the failure curve of the base material, b) Damage evolution of the critical elements with and without defined pre-damage

With the definition of a pre-damage value D_{ini} , the damage evolution in the critical element can be calculated according to Eq. 1. In this equation $\Delta\varepsilon_{pl}$ equals the plastic strain increment for each time step, and $\varepsilon_f(\eta)$ equals the failure strain for the stress state at the corresponding time step.

$$D(\Delta\varepsilon_{pl}) = D_{ini} + \sum \frac{\Delta\varepsilon_{pl}}{\varepsilon_f(\eta)} \quad (1)$$

In order to achieve element failure for a locally critical plastic strain ε_{crit} the accumulated damage value D has to be equal to 1. By rearranging Eq. 1, the value for D_{ini} can be directly calculated from the load paths of the critical elements (Eq. 2).

$$D_{ini} = 1 - \sum_0^{\varepsilon_{crit}} \frac{\Delta\varepsilon_{pl}}{\varepsilon_f(\eta)} \quad (2)$$

The results of these calculations can be seen in Fig. 5b. The solid lines show the damage evolution in the critical elements without the consideration of any pre-damage. The dashed lines show the damage evolution with the consideration of pre-damage. It can be seen that the necessary pre-damage is equal for the two different test types. This means that the required pre-damage is independent of the stress state of the respective test. The calculated pre-damage value can be defined as a history variable with the keyword `*INITIAL_STRESS_SHELL_SET`. In order to validate the approach the tensile and punch tests with specimens with a hole due to self-piercing riveting have been simulated with the modeled notch zone for which the calculated damage values have been defined. The results of these simulations are shown in Fig. 6. In Fig. 6a, the load paths of the critical elements within the modeled notch zone are plotted. It can be seen, that element failure occurs before the load paths cross the failure curve of the base material. This is a direct result of the defined pre-damage, which results in an earlier element failure. A comparison between the experimental results of the tensile and punch tests with the simulation results shows a good agreement (Fig. 6b and c). For both tests, the simulation is able to match the maximum forces as well as the overall characteristics of the specimen behavior. It can thus be shown that the proposed method is able to reproduce specimen failure due to geometrical notch effects.

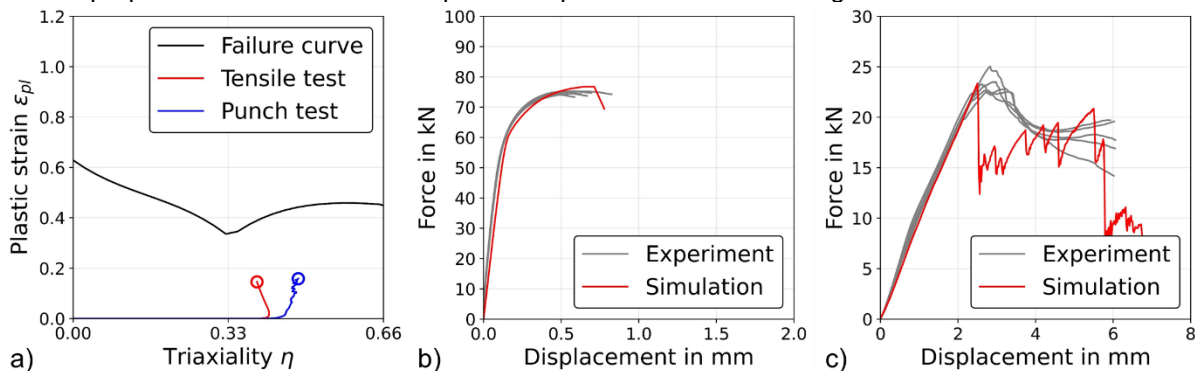


Fig.6: a) Load paths for the critical elements for the tensile and punch tests with defined pre-damage, b) Comparison between the experimental results of the tensile test with hole due to self-piercing riveting and the simulation, c) Comparison between the experimental results of the punch test with hole due to self-piercing riveting and the simulation

3.2 Metallurgical notch at resistance-welding elements

Similar to the methodology for geometrical notches presented in chapter 3.1, the approach for the metallurgical notches is based on an explicitly modeled notch zone as well. Within this notch zone, the flow and failure behavior of the base material is adjusted in order to match the material behavior of the SHAZ. This approach is similar to the procedure that has been used in [7] to simulate the effect of SHAZs in press-hardened steel due to spot welding. For the experimentally investigated tensile and punch tests with SHAZ due to resistance element welding shell models with an explicitly modeled SHAZ have been created. The models can be seen in Fig. 7. In order to take the lower strength of the SHAZ into account, the flow curve of the base material was scaled by 0.8 for the SHAZ based on a comparison with the experimental force vs. displacement curves of the tensile test specimens with SHAZ. This is necessary in order to be able to model the strain localization in the SHAZ. The flow curve of the base material as well as the scaled flow curve of the SHAZ can be seen in Fig. 8a. In the next step, the tensile and punch tests have been simulated with the scaled flow curve and without the consideration of

element failure in order to obtain the load paths of the critical elements within the modeled SHAZ. The results of these investigations can be seen in Fig. 8b. Based on these results the failure curve of the base material is adjusted in order to match the experimental force vs. displacement behavior of the tensile and punch specimens with SHAZ.

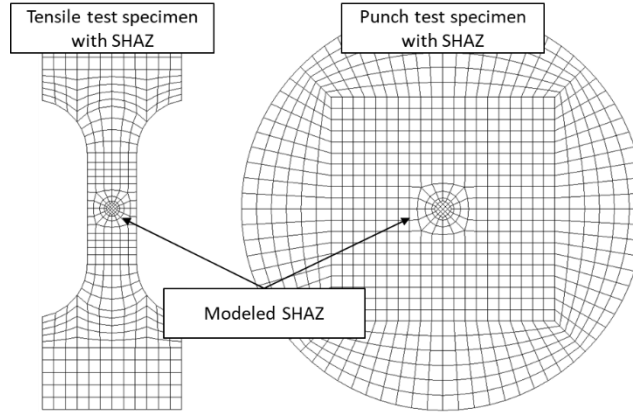


Fig.7: FE-models of the tensile and punch specimens with a modeled SHAZ due to the resistance element welding process

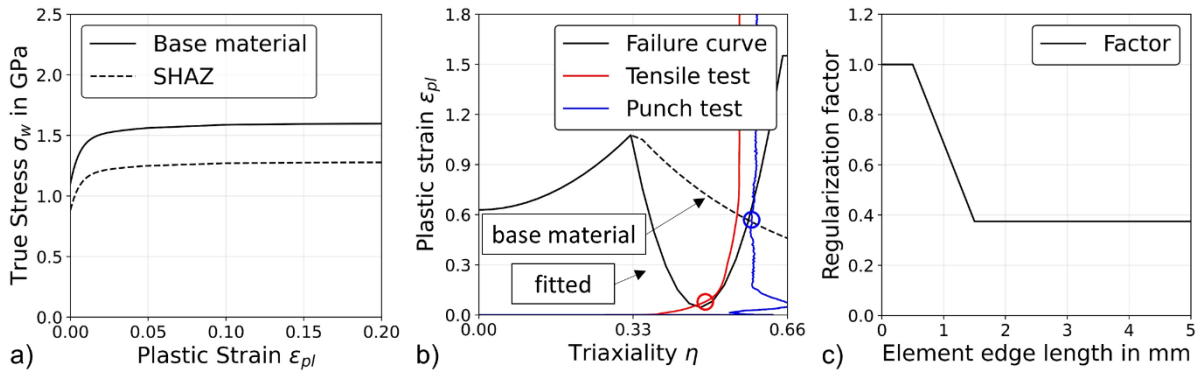


Fig.8: a) Flow curves for the base material and the SHAZ, b) Failure curve of the base material and fitted failure curve for the SHAZ, c) Regularization factor for the SHAZ

In order to adapt the failure curve of the base material to the behavior of the SHAZ, a quadratic approach as defined in Eq. 3 has been used. Only the part of the failure curve where $\eta \geq \frac{1}{3}$ has been adapted. The rest of the failure curve was left unchanged.

$$\varepsilon_f = d_1 + d_2(\eta - d_3)^2 \quad (3)$$

The Parameter d_2 of the approach is fixed so that the two branches of the failure curve have the same value for $\eta = \frac{1}{3}$. The free parameters d_1 and d_3 of the approach can be found based on the strain paths of the critical elements and the deviation from the critical plastic strain, which is necessary to match the global specimen behavior in the simulation. This results in an optimization problem (Eq. 4), which can be solved based on the strain paths of the critical elements shown in Fig. 8b.

$$\min_{d_1, d_3} \sum_N |D(\Delta\varepsilon_{pl}) - 1| \quad (4)$$

The fitted shape of the failure curve for the SHAZ can be seen in Fig. 8b. To reduce the influence of the element edge length on the results of the simulation, a regularization curve is used. The shape of this regularization curve can be found in Fig. 8c. With the adjusted flow and failure behavior for the SHAZ, the tensile and punch tests have been simulated. The results of these simulations can be found in Fig. 9. In Fig. 9a, the load paths of the critical elements within the SHAZ are plotted as well as the adjusted failure curve that is regularized according to the used element length (1.5 mm). A comparison between the experimental results of the tensile and punch tests and the simulations can be found in Fig. 9b and c. Overall the calculated force vs. displacement curves show a good correlation with the experiments and the global behavior of the specimens can be matched.

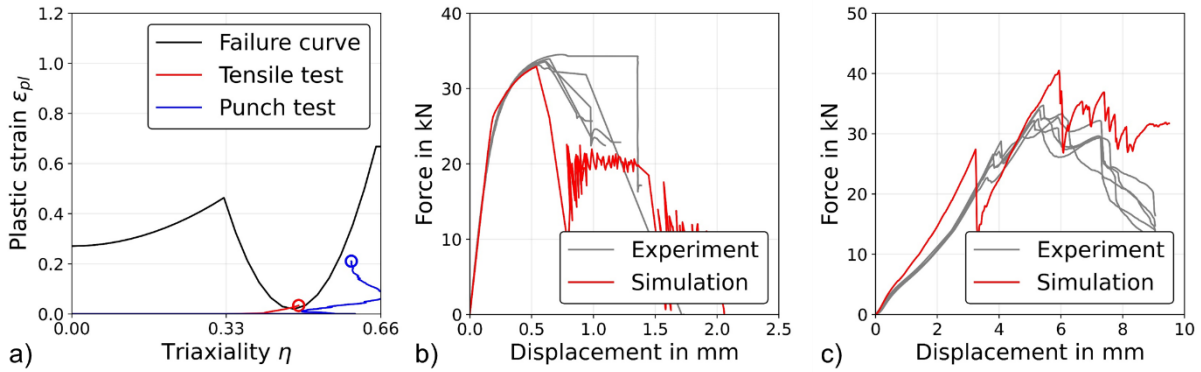


Fig.9: a) Load paths for the critical elements in the modeled SHAZ for the tensile and punch loading, b) Comparison between the experimental results of the tensile test simulation, c) Comparison between the experimental results of the punch test simulation

3.3 Load bearing capacity

The load bearing capacity of the joint itself is modeled with the help of the ***CONSTRAINED_SPR3** (model 2) model. The ***CONSTRAINED_SPR3** (model 2) model is based on an element free approach, which includes the load bearing and failure behavior of the joint based on constraints between the shell nodes of the connected parts. In Fig. 10b a schematic representation of the **CONSTRAINED_SPR3** (model 2) model can be seen. The blue marked rivet node defines the position of the joint. All of the shell nodes on the slave and master side of the connection within the domain of influence are automatically tied together with constraints. The ***CONSTRAINED_SPR3** (model 2) model is placed in the center of the shell model of the LWF-KS-2-specimens, which can be seen in Fig. 10a. The parameters of the ***CONSTRAINED_SPR3** (model 2) model are calibrated based on the experimental results of the LWF-KS-2-specimen tests.

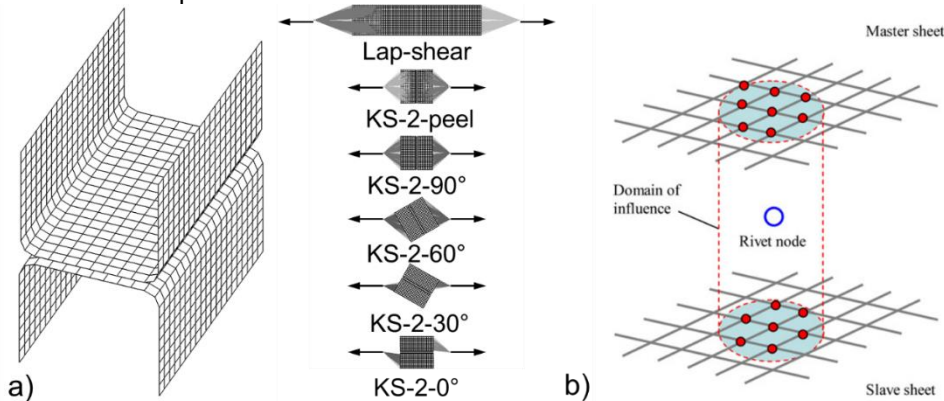


Fig.10: a) Simulation model of the LWF-KS-2-specimens under varying load angles, b) Illustration of the ***CONSTRAINED_SPR3** (model 2) model with the rivet node, the domain of influence and the mesh nodes on the slave and master side which are constrained [8]

In Fig. 11 the simulation results with the ***CONSTRAINED_SPR3** (model 2) model for the self-piercing riveted joint are compared to the experimental results. The model shows a good correspondence of the load bearing behavior with the experimental results for the investigated load angles. Deviations between the experiment and the simulation can be found for the LWF-KS-2-0°-specimen as well as the lap-shear specimen. The deviations for the LWF-KS-2-0°-specimen can be explained by the experimental behavior of the specimen. In the experiment, the joint fails due to tearing of the aluminum sheet. This cannot be covered by the simulation due to the lack of a validated failure model for the aluminum alloy. For the lap-shear specimen an overestimation of the load bearing capacity in the simulation can be observed. This overestimation occurs due to the procedure of the parameter determination. The parameters, which govern the load bearing capacity of the model under shear load, have been calibrated based on the LWF-KS-2-specimen. Since the model is unable to describe the local load situation at the rivet for the lap-shear specimen, this procedure results in an overestimation of the maximum load for the lap-shear specimen. For the remaining specimens the simulations show a good correlation with the experimental results regarding the maximum loads as well as the displacements at fracture.

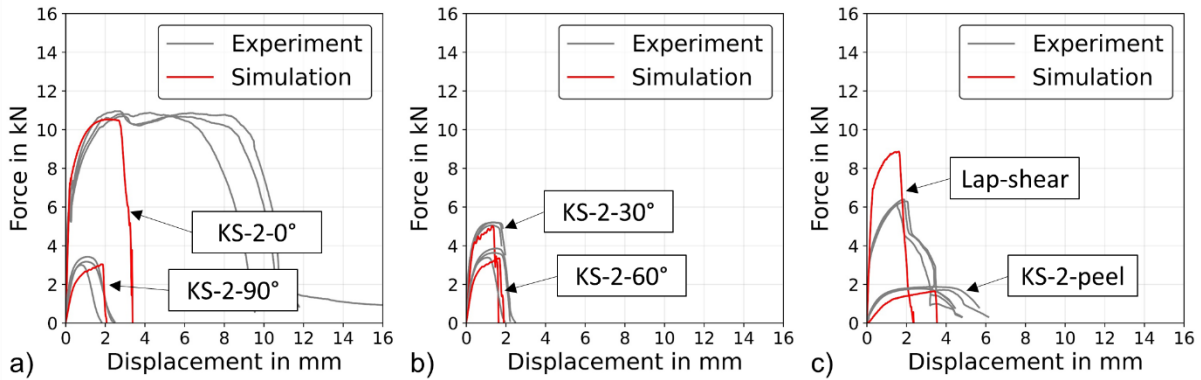


Fig.11: Simulation results with the **CONSTRAINED_SPR3 (model 2)* model for the self-piercing riveted joint in comparison with the experimental results (a. LWF-KS-2-0° and LWF-KS-2-90°, b. LWF-KS-2-30° and LWF-KS-2-60°, c. LWF-KS-2-peel and lap-shear specimen)

In Fig. 12 the simulation results with the **CONSTRAINED_SPR3 (model 2)* model for the resistance element welded LWF-KS-2-specimens tests are compared with the experiments. The simulated results show a very good agreement with the experimental results for the tensile (LWF-KS-2-90°) and shear (LWF-KS-2-0°) loading as well as for the mixed loading angles LWF-KS-2-30° and LWF-KS-2-60°. Furthermore, the experimental behavior of the LWF-KS-2-peel and the lap-shear specimen can be reproduced as well. It can be seen that the differences between the experimental maximum force for the lap-shear specimen and the results of the simulation are less pronounced compared to the self-piercing riveted joint. This is a direct result of the parameter calibration for the load bearing capacity under shear loading. The load bearing capacity under shear loading was adjusted to the lower force level of the LWF-KS-2-0° specimens of approximately 7 kN. This corresponds with the load bearing capacity of the lap-shear specimen. Hence, the force vs. displacement behavior of the two different specimens can be matched.

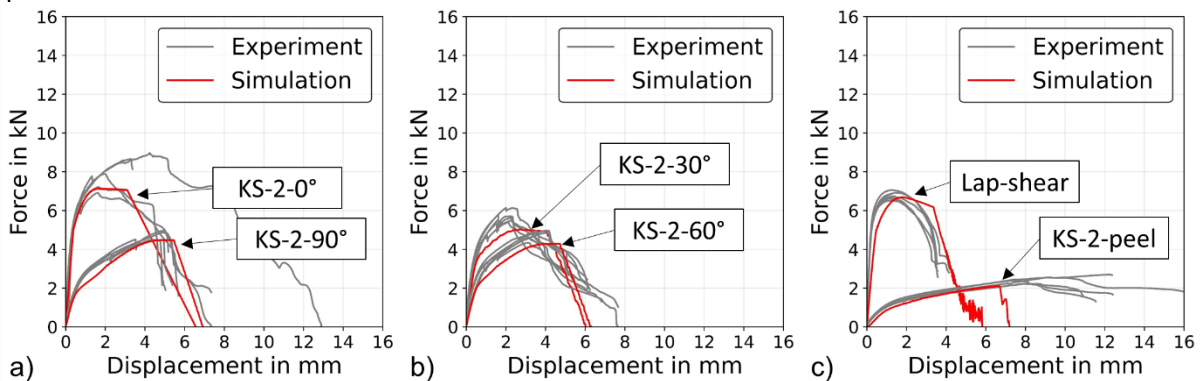


Fig.12: Simulation results with the **CONSTRAINED_SPR3 (model 2)* model for the resistance element welded joint in comparison with the experimental results (a. LWF-KS-2-0° and LWF-KS-2-90°, b. LWF-KS-2-30° and LWF-KS-2-60°, c. LWF-KS-2-peel and lap-shear specimen)

4 Validation on component level

In order to validate the modeling techniques for the consideration of notch effects presented in section 3.1 and 3.2 under complex loading conditions, simulations of component tests have been performed. The simulation model that has been used to simulate component test can be seen in Fig. 13. The component is a closed profile with a self-piercing rivet respectively resistance-welding element on the side opposite of the stamp of the three point bending test set up. Therefore, the notch due to the joint is situated in the position with the highest bending moment and is thus subjected to a tensile load in plane of the sheet metal. The notch zones are modeled with the approaches presented in chapter 3.1 and 3.2, the joints themselves are modeled with the **CONSTRAINED_SPR3 (model 2)* models from chapter 3.3. The results of the component simulations are compared to the experimental results regarding the force vs. displacement curves as well as the overall failure mechanism.

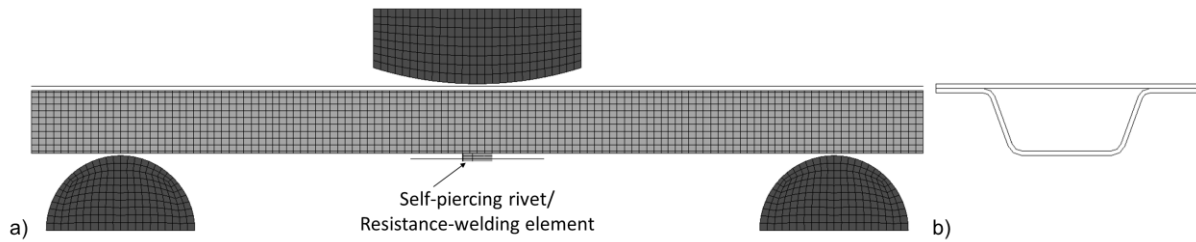


Fig. 13: a) Simulation model of the component test under three point bending, b) Cross-section of the investigated profile

The simulation results for the component test with a geometrical notch due to self-piercing riveting can be seen in Fig. 14. Overall, there is a good correlation between the experimentally measured and calculated force vs. displacement curves. The simulation is able to reproduce the experimental load bearing capacity of the specimen as well as the displacement at failure (Fig. 14a). A comparison of the fracture patterns shows that the simulation is able to capture component failure due to the induced notch. It can be seen that the strain localizes at the edge of the modeled hole, which subsequently leads to the crack initiation. The crack propagates tangentially from the edge of the hole, which finally leads to the failure of the component (Fig. 14c). This fracture pattern corresponds to the experimental result, which can be seen in Fig. 14b. It can be shown that the approach described in section 3.1 is able to capture component failure due to geometrical notches under complex loading conditions.

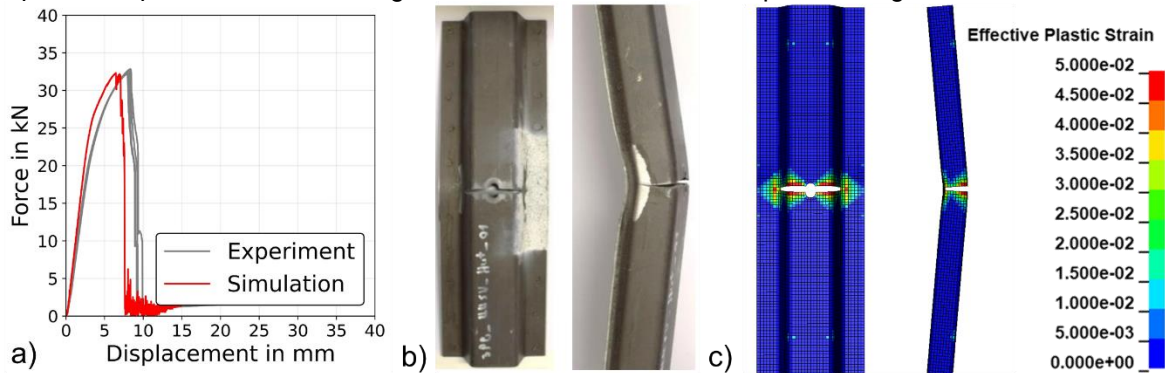


Fig. 14: a) Comparison of the calculated force vs. displacement curves with the experimental results for the self-piercing riveted component, b) Experimental fracture pattern, c) Simulated fracture pattern with strain distribution

The results of the simulations for the component with metallurgical notch due to resistance element welding can be seen in Fig. 15. A comparison of the calculated force vs. displacement curves with the experimental results shows a good correlation, although the maximum force as well as the displacement at failure are slightly underestimated by the simulation (Fig. 15a). The cause of this underestimation of the average maximum force and the displacement at failure can be found in the geometrical overestimation of the real dimensions of the SHAZ due to the coarse mesh that has been used. This overestimation leads to a strong weakening of the component and thus an increased localization in the modeled SHAZ and an early fracture. A comparison of the calculated fracture pattern with the experimental results shows a good correlation (Fig. 14b and c). In both cases, the strain localizes in the SHAZ due to the locally reduced material strength. In the following, this leads to a crack initiation in the SHAZ. The crack propagates from the SHAZ into the base material, which finally leads to the failure of the component. Therefore, the calculated failure mechanism for the component is in agreement with the experimental observation. The simulation is able to predict component failure due to the metallurgical notch.

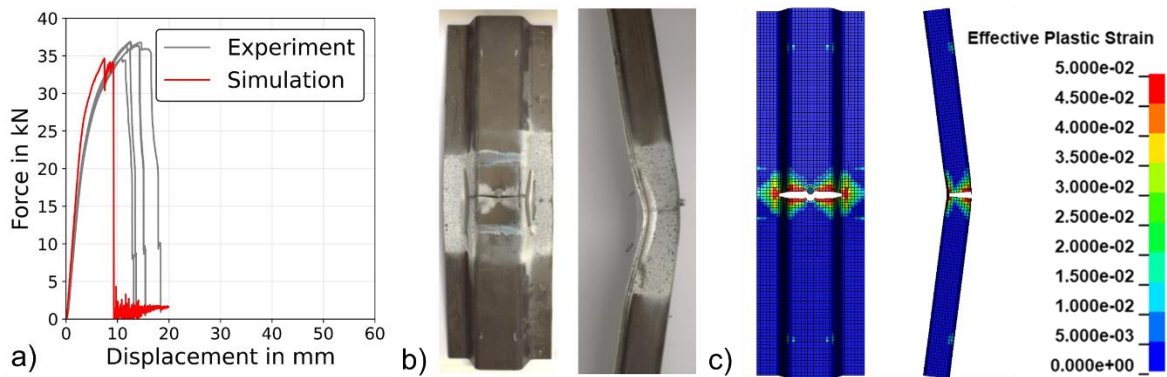


Fig. 15: a) Comparison of the calculated force vs. displacement curves with the experimental results for the resistance-element welded component, b) Experimental fracture pattern, c) Simulated fracture pattern with strain distribution

5 Summary

In this paper, two modeling approaches for geometrical and metallurgical notches have been presented that are able to predict component failure due to notch effects at joints. Both approaches are based on an explicitly modeled notch zone. For the geometrical notches, a hole in the area of the joint is modeled with a surrounding area of elements for which a pre-damage has been defined. The value for this pre-damage has been calculated based on the load paths of the critical elements in the notch zone and a comparison with the experimental results. For the metallurgical notches, a SHAZ has been modeled for which the flow and failure behavior of the base material have been adjusted in a way that it is possible to capture the reduced strength of the SHAZ. Furthermore `*CONSTRAINED_SPR3` (model 2) models have been calibrated based on the experimental results of the LWF-KS-2-specimens in order to include the load bearing behavior of the joint itself. The calibrated modeling approaches have been validated on component level. Therefore, simulation models of the component test set up have been created in which the corresponding modeling approaches have been included. The results of the component simulations have been compared with the experimental results. It can be shown that the developed modeling techniques are able to predict component failure due to notch effects under complex loading conditions.

6 Acknowledgement

The IGF research project 19751 N by the Forschungsvereinigung Stahlanwendung e.V. (FOSTA) has been funded by the AiF under the program for promotion of industrial research (IGF) by the Federal Ministry of Economics and Energy based on a decision of the German Bundestag. The authors would like to thank all parties involved in the funding and the support of this research project. The results of this research project will be published in form of a final report via the Forschungsvereinigung Stahlanwendung e.V. (FOSTA) shortly after the end of the project.

7 Literature

- [1] Seeger, F.; Feucht, M.; Dumitru, G.; Graf, T.: Enhancement of Spot Weld Modeling using MAT_100_DAI, 7. LS-DYNA Anwenderforum, 2008
- [2] Bier, M.; Sommer, S.: Simplified modeling of self-piercing riveted joints for crash simulation with a modified version of `*CONSTRAINED_INTERPOLATION_SPOTWELD`, 9th European LS-DYNA Conference, 2013
- [3] Hahn, O.; Gieske, D.; Rhode, A.: Probe und Probenstanzvorrichtung zum Einsatz in Zugmaschinen, Patentschrift DE 195 22 247 A1, 1996
- [4] Sommer, S.; Bähr, P.; Meschut, G.; Unruh, E.: Charakterisierung und Modellierung von Kerbeffekten durch Mischverbindungen in Karosseriebauteilen aus höchstfesten Stählen, final report for AiF-FOSTA-project P1268 IGF-No. 19751N, to be published
- [5] DVS Merkblatt 3480: Prüfung von Verbindungseigenschaften - Prüfung der Eigenschaften mechanisch und kombiniert mittels Kleben gefertigter Verbindungen, Deutscher Verband für Schweißen und verwandte Verfahren e.V., 2017
- [6] DIN EN ISO 12004: Metallische Werkstoffe – Bleche und Bänder – Bestimmung der Grenzformänderungskurve, Deutsches Institut für Normung e.V., 2019

- [7] Gumbsch, P.; Sommer, S.; Burget, S.; Roos, E.; Wink, H.-J.; Krätschmer, D.; Hahn, O.; Meschut, G.; Klokkers, F.; Hein, D.: Charakterisierung und Ersatzmodellierung des Bruchverhaltens von Punktschweißverbindungen aus ultrahochfesten Stählen für die Crashsimulation unter Berücksichtigung der Auswirkung der Verbindung auf das Bauteilverhalten, final report for AiF-FOSTA-project A 262 / P 806, 2013
- [8] Hanssen, A.G.; Olovsson, L.; Porcaro, R.; Langseth, M.: A large-scale finite element point-connector model for self-piercing rivet connections, *European Journal of Mechanics A/Solids* 29, 2010